

Numerical Analysis of Shape Stability of Rubber Boot

David Samek, Jakub Javorik

Abstract—This paper presents numerical models that are able to simulate a buckling of the rubber boot. Rubber boot must be able of a large change of its length. A buckling of cylindrical shape of the boot during this deformation would cause a serious problem. Due to the space limitation in an assembly it is quite difficult to find optimal shape of the boot profile which will be able of the required deformation without the buckling. We have created numerical models that are able to simulate mechanical behavior of the compressed boot including the buckling of the boot with an inappropriate profile. Due to the material of the boot (rubber), a nonlinear hyperelastic material model was used in the analyses. The material constants of this hyperelastic model were obtained from the uniaxial and equibiaxial tests of the boot material. Created numerical models were used to design the optimal shape of the boot which eliminates the risk of the buckling.

Keywords—boot, buckling, hyperelasticity, numerical analysis, rubber.

I. INTRODUCTION

THE rubber has irreplaceable role in many industrial applications today [1]-[3]. A boot protecting moving mechanical parts can be considered as one of such products. In these cases, the rubber seems to be the best, and often the only appropriate material. Although there are several limiting factors that may cause contradictions. The boot must be sufficiently rigid to maintain its shape, but it must not be too rigid to be capable of the required deformation and dimensional changes with the moving mechanism.

In our case, there are also some other restrictions (mainly in size) caused by a small space that is available in the construction. The shape and dimensions of the boot (especially its folds) are very important for its proper function. It can be very difficult to find the correct shape of the product, if any of these parameters is limited. A numerical analysis is a very useful tool to solve these problems [4]-[16].

The goal of presented work was to find optimal shape of the rubber boot that will satisfy all size limitation and as well as it will be able of required deformation (i.e. compression in longitudinal direction) of the boot.

D. Samek is with the Department of Production Engineering, Tomas Bata University in Zlin, nam. T. G. Masaryka 5555, 760 01 Zlin, Czech Republic (e-mail: samek@ft.utb.cz).

J. Javorik is with the Department of Production Engineering, Tomas Bata University in Zlin, nam. T. G. Masaryka 5555, 760 01 Zlin, Czech Republic (phone: +420 576 035 151; fax: +420 576 035 176; e-mail: javorik@ft.utb.cz).

II. MATERIAL AND METHODS

A. Rubber Boot Geometry and Material

The cylindrical rubber boot which must be able to reduce its length to about half of the original length is the object of the analysis (Fig. 1).

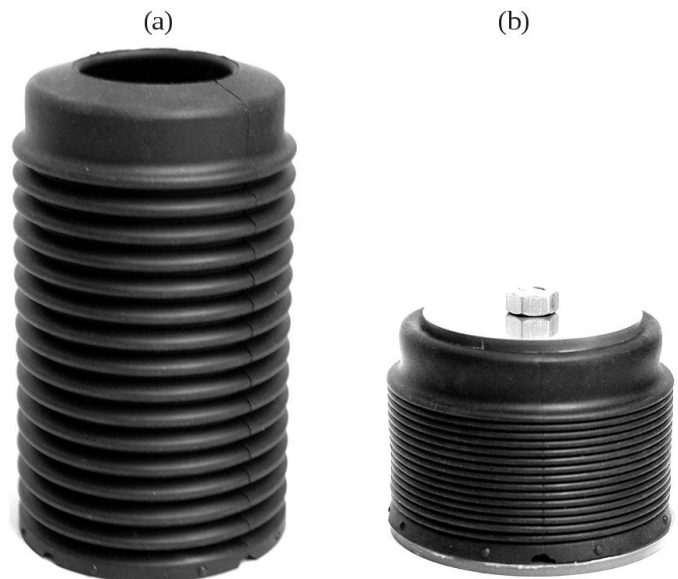


Fig. 1 original shape of boot in unloaded state (a) and after compression (b)

Boot is made of Styrene Butadiene Rubber [17]-[18]. Its length is 133 mm and outer diameter is 77 mm. The original shape of the profile of boot is shown in Fig. 2; dimension $h = 0.4$ mm. The folds of boot are problematic aspect of the part, particularly the thickness h in the narrowing of the profile folds.

Boot with profile from Fig. 1 and 2 is efficient in terms of its ease and correct deformation under a compression. However, the small thickness h causes low strength in the folds tops that leads to the failures of boot during a cyclic loading. Due to space limitations in the boot vicinity, the number of folds or the height z can not be changed ($z = 4.75$ mm, 15 folds). Therefore, the thickness h remains as only parameter that can be changed. But if the thickness increases largely then the boot becomes too rigid, and is no longer operational, it means that when it is compressed it loses shape stability and collapses to unacceptable shape (Fig. 3). Fig. 3 shows the real

product of $h = 1.8$ mm. The task is to find the maximum thickness h , at which the boot is still able to deform without the shape collapse (without the buckling).

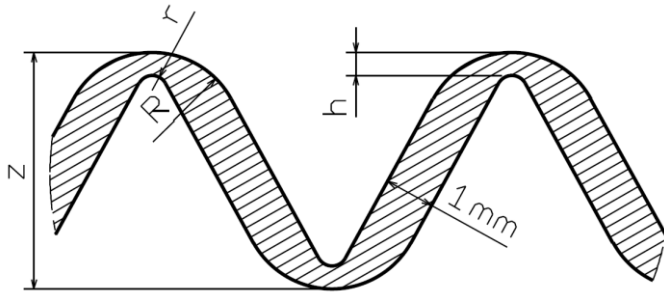


Fig. 2 boot profile



Fig. 3 buckling of the boot with an inappropriate profile ($h=1.8$ mm)

B. Material Model

With a given product we can expect both large displacement and large deformation (tens of percent). Furthermore, we know that the relationship between stress and strain will be strongly nonlinear in the case of a rubber [19]-[26]. Due to these facts a hyperelastic nonlinear material model must be used. Currently,

there are a number of hyperelastic models [27]-[33] and many of them are implemented in systems using the finite element method (FEM). Current hyperelastic models are based on the strain energy function W [34]-[36]. If we define this function, we can derivate the stress value S_{ij} from this function by corresponding components of the deformation tensor C_{ij} , as is described in (1).

$$S_{ij} = 2 \frac{W}{C_{ij}} \tag{1}$$

The James-Green-Simpson (or 3rd order deformation) hyperelastic model appeared to be the most appropriate for the material of the boot. The reasons for this choice are explained below. This model defines the strain energy density function W as

$$W = c_{10}(J_1 - 3) + c_{01}(J_2 - 3) + c_{11}(J_1 - 3)(J_2 - 3) + c_{20}(J_1 - 3)^2 + c_{30}(J_1 - 3)^3 \tag{2}$$

where the c_{ij} coefficients are material constants determined from experimental data, and J_1 and J_2 are first and second invariant of the right Cauchy-Green deformation tensor. If this tensor is expressed by principal components of stretch ratio λ , then it can be written as follows

$$C_{ij} = \begin{bmatrix} \lambda_1^2 & 0 & 0 \\ 0 & \lambda_2^2 & 0 \\ 0 & 0 & \lambda_3^2 \end{bmatrix} \tag{3}$$

and first and second invariant of this tensor J_1 and J_2 are

$$J_1 = \lambda_1^2 + \lambda_2^2 + \lambda_3^2 \tag{4}$$

$$J_2 = \lambda_1^2 \lambda_2^2 + \lambda_2^2 \lambda_3^2 + \lambda_3^2 \lambda_1^2 \tag{5}$$

For accurate determination of material constants c_{ij} used in (2) it is necessary to test elastomer in typical deformation modes. They are: a uniaxial tension (Fig. 4a), equibiaxial tension (Fig. 4b) and pure shear (or planar tension) (Fig. 4c) [37]-[43]. We used data from uniaxial and equibiaxial tension tests for our model.

1) Uniaxial Tension Test

The uniaxial tensile test was carried out on a universal tensile testing machine according to ISO 37. Specimens of 1A type with the thickness of 1 mm were used (Fig. 5). Stress/strain curve was measured during the whole range of loading. Specimens were loaded up to their break.

2) Equibiaxial Tension Test

This test is specific for elastomers and therefore it is less frequent. Due to these reasons it is not standardized and such

tests are rarely performed in industrial laboratories.

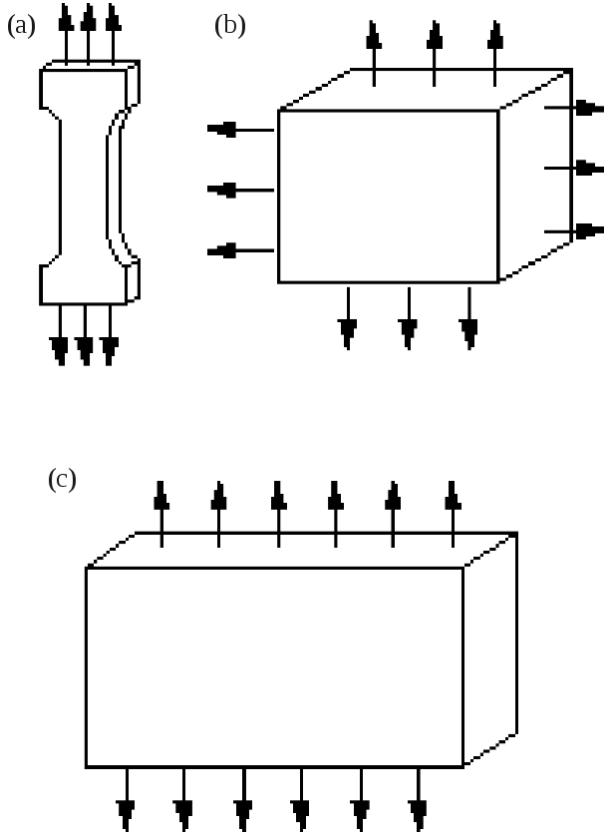


Fig. 4 schematics of three basic tests of mechanics of elastomers: uniaxial tension (a), equibiaxial tension (b) and pure shear (c)



Fig. 5 1A type of uniaxial tension test specimen (according to ISO 37)

The principle of the test is to stretch flat specimen in all directions of its surface. There are several methods to load the specimen in this way. We used method of flat circular specimen inflation that is called as a "Bubble Inflation Technique" [44]-[45]. In this method a uniform circular specimen of elastomer is clamped at the rim and inflated using compressed air to one side (Fig. 6 and 7). The specimen is deformed to the shape of bubble. The inflation of the specimen results in an equibiaxial stretching near the pole of the bubble and in the planar tension near the rim. The inflation of the specimen and current value of pressure is recorded in short time intervals.

Obtained stress-strain relations for uniaxial and equibiaxial tension of boot material are shown in Fig. 8. We can see the suitability of the James-Green-Simpson hyperelastic material model that is able to predict behavior of the boot material with

minimal deviation from the experiment.

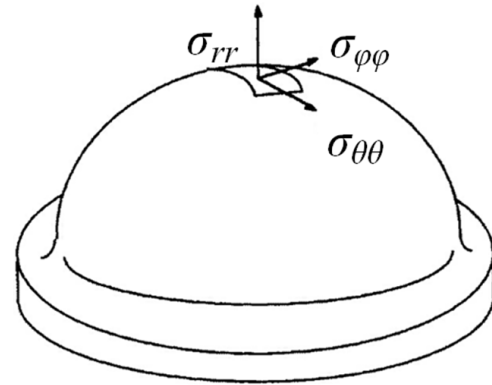


Fig. 6 bubble inflation technique

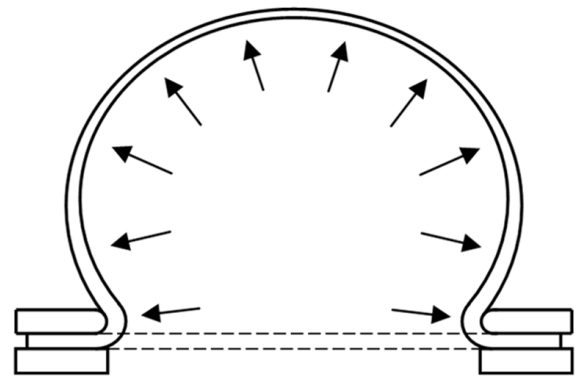


Fig. 7 the specimen inflation

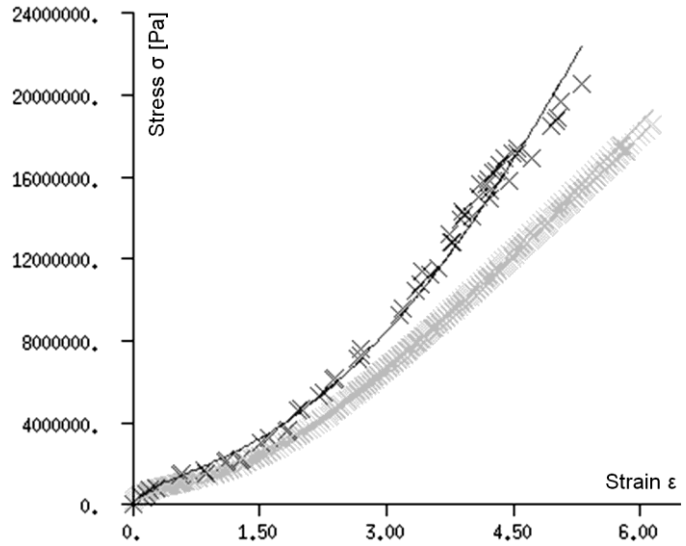


Fig. 8 stress-strain diagram of experimental data and hyperelastic material model (James-Green-Simpson); gray – uniaxial tension, black – equibiaxial tension, cross – experiment, line – model

Stress in the specimen can be calculated from the pressure p

inside the bubble, initial specimen thickness t_0 and the stretch ratio λ . Thanks to the spherical symmetry we can consider $\sigma_{\theta\theta}=\sigma_{\phi\phi}$ at the pole of the bubble. Then we can write the Cauchy stress tensor in spherical coordinates as:

$$\sigma = \begin{bmatrix} \sigma_{rr} & 0 & 0 \\ 0 & \sigma_{\theta\theta} & 0 \\ 0 & 0 & \sigma_{\theta\theta} \end{bmatrix}_{(r,\theta,z)} \quad (6)$$

The thickness of specimen is small and the ratio between the thickness of the inflated specimen t and the curvature radius r is small enough, then the thin shell assumption allow us to neglect the radial stress σ_{rr} in front of the stress $\sigma_{\theta\theta}$. In addition we equate $\sigma_{\theta\theta}$ to the thickness-average hoop stress, which leads to:

$$\sigma_{\theta\theta} = \frac{pr}{2t} \quad (7)$$

where p is the differential inflation pressure, r is curvature radius of specimen and t is the specimen thickness.

With consideration of material incompressibility we can express the thickness of inflated specimen t as:

$$t = \frac{t_0}{\lambda_{\theta\theta}^2} \quad (8)$$

where t_0 is the initial thickness of specimen (unloaded state). Further we have to measure the stretch $\lambda_{\theta\theta}$ at the pole of inflated material. Generally stretch λ is the ratio between the current length l and the initial length l_0 :

$$\lambda = \frac{l}{l_0} \quad (9)$$

We can use some of optical method for measurement of stretch $\lambda_{\theta\theta}$ and curvature radius r (camera, video camera, laser, digital image correlation - DIC etc.). The white strips were drawn in the central area of specimen for stretch measurement (Fig. 9). It is important to measure elongation and curvature radius only in the area near to pole (between the strips) of inflated specimen and not on entire bubble contour because only on the pole the equibiaxial state of stress occurs. Substituting (8) into (7) we can compute the hoop stress $\sigma_{\theta\theta}$ as:

$$\sigma_{\theta\theta} = \frac{pr\lambda_{\theta\theta}^2}{2t_0} \quad (10)$$

C. Numerical FEM Model

Due to the fact that the model must be able to simulate buckling, shown in Fig. 3, it must be created as a three-dimensional solid - despite the fact that its original unloaded shape is axisymmetric. There can not be used shell elements whereas the thickness of boot is not uniform and just the

influence of different thickness in folds on behavior of the component was evaluated. Therefore 3D elements of "TETRAHEDRON" type were used to create the FEM model. A quarter symmetry of the collapsed shape of boot is apparent from Fig. 3. This fact allows us to reduce the model geometry only to one quarter. The resulting model geometry is then shown in Fig. 10.



Fig. 9 equibiaxial tension test

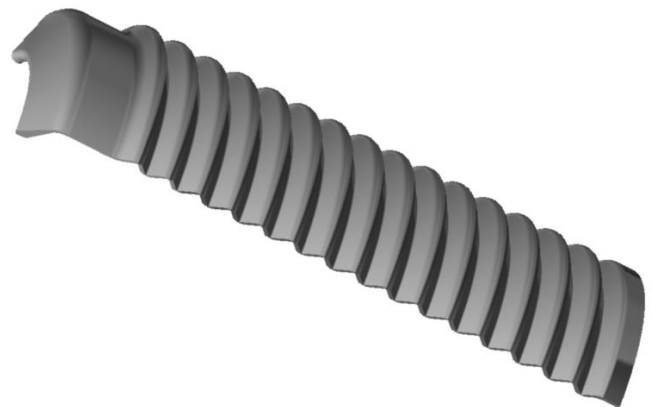


Fig. 10 geometry of FEM model

Five models with different boot profiles were created. The model of already existing boot that collapses under the pressure (Fig. 3) was created and its profile is shown in the Fig 11. The size of $h=1.8$ mm is greater than the thickness of the boot wall (1 mm) in this model. The purpose was to verify the accuracy of the FEM model and mainly its ability to simulate buckling of the real rubber boot. The profile of this model is the only which is not symmetric. It means that the size $h=1.8$ mm is only in the inner folds of profile; and different value of $h=1$ mm is in the outer folds (Fig. 11). All other created

models have symmetric profile with the same value of h in inner and outer folds.

Next reference model was the model with a minimum thickness $h=0.4$ mm (Fig. 12). We also knew that this geometry is able to deform correctly but such product has insufficient strength (Fig. 1) and it fails just in this points (i.e. boot folds). Therefore we need to find the maximum of h with which there is no buckling of the boot. For this purpose three other models were created; they dimensions h are: 0.6 mm (Fig. 13), 0.8 mm (Fig. 14) and 1.0 mm (Fig. 15). As the radius r in all three models has constant value 0.3 mm, different dimensions h will be achieved only by changing the radius R (Fig. 2) in these models.

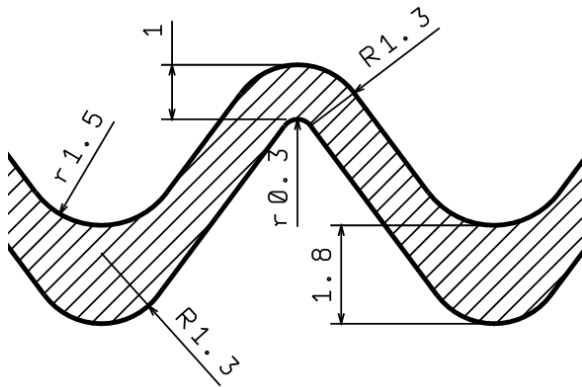


Fig. 11 profile of model with size $h=1.8$ mm

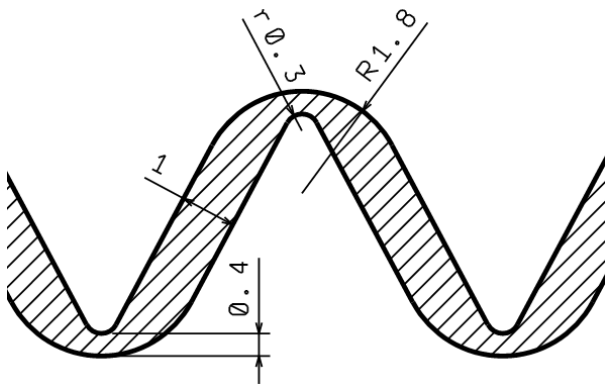


Fig. 12 profile of model with size $h=0.4$ mm

Material constants for the most used hyperelastic models (Neo-Hookean, Mooney-Rivlin, Yeoh, Signiorini, James-Green-Simpson, Ogden, Arruda-Boyce, and Gent [46]-[50]) were determined from the test results. James-Green-Simpson model (2) showed the smallest error (the smallest deviation from the experimental stress/strain curves) and therefore was chosen for the FEM model.

Material constants for James-Green-Simpson model determined from the tests are as follows (in MPa): $c_{10}=429321$; $c_{01}=-14574$; $c_{11}=220.2$; $c_{20}=15554$; $c_{30}=-84.2$. The least squares method was used to determine constants of

hyperelastic models from the experimental results.

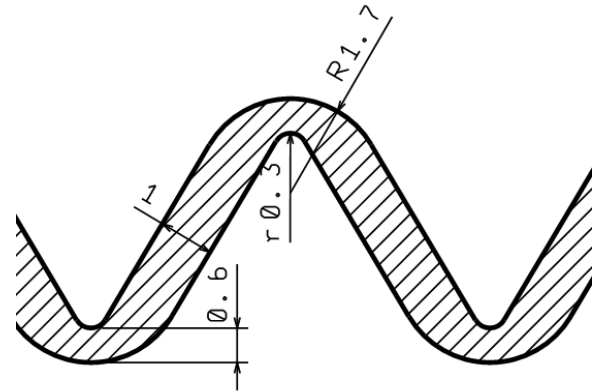


Fig. 13 profile of model with size $h=0.6$ mm

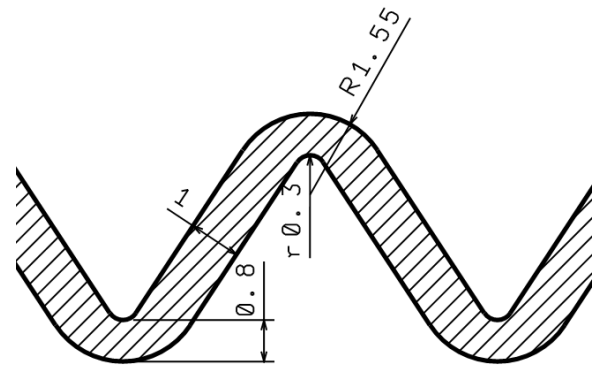


Fig. 14 profile of model with size $h=0.8$ mm

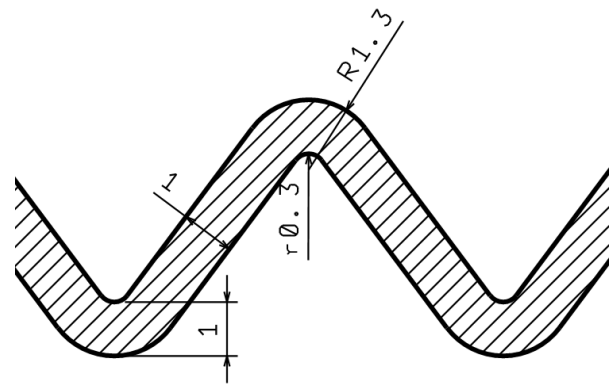


Fig. 15 profile of model with size $h=1.0$ mm

III. RESULTS

Results of the analysis of the original functional boot shape from Fig. 1 are shown in Fig. 16. Figure shows the deformation of boot with a dimension $h=0.4$ mm after a maximum compression value of 53 mm. Buckling occurs if the compression will be larger than 53 mm.

Opposite extreme, i.e. deformation of model with $h=1.8$

mm, is illustrated in Fig. 17. In this case the buckling occurs already after the small compression of 23 mm. The collapsed shape of the model corresponds exactly with the real product shown in Fig. 3.

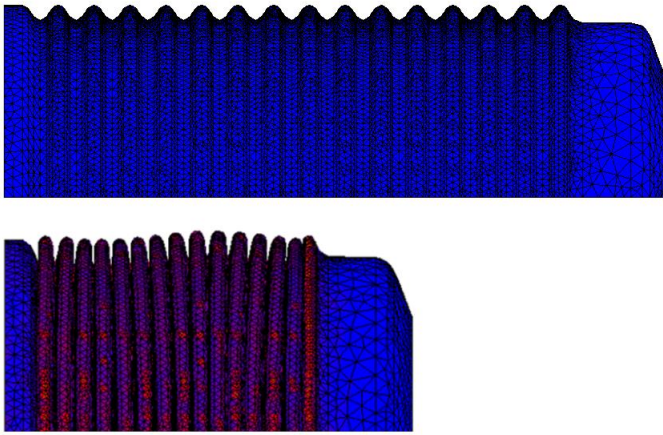


Fig. 16 deformation of model with $h=0.4$ mm

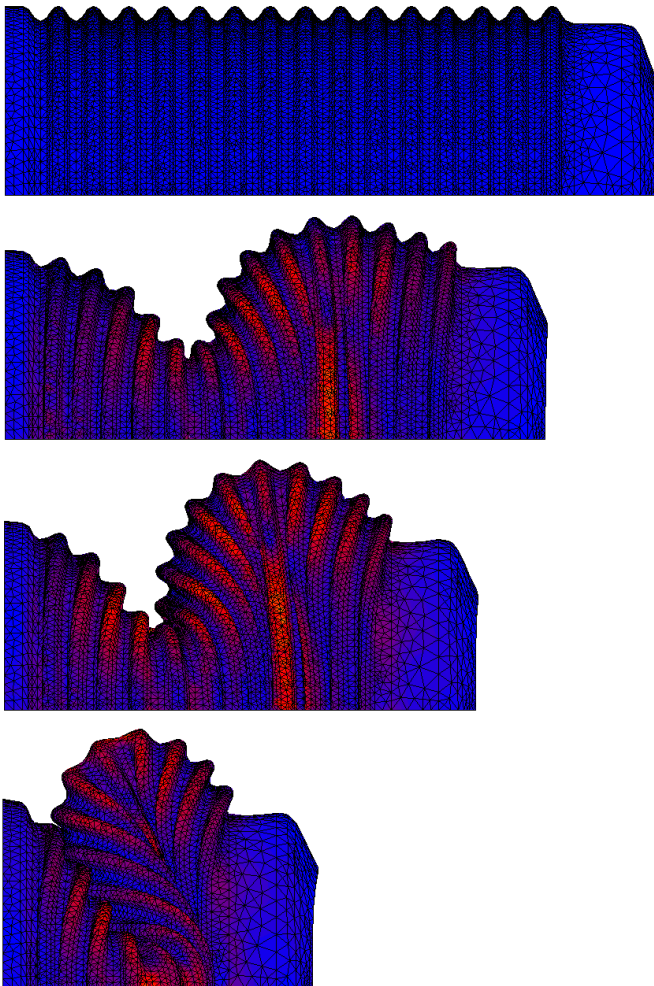


Fig. 17 deformation of model with $h=1.8$ mm

Values of compression (evaluated by displacement of right end of boot in mm) which will trigger a collapse were monitored as well as for the other three models ($h=0.6$ mm, 0.8 mm and 1.0 mm). These values are listed in Table I, and the relation between the h size of analyzed models and these values is shown in Fig. 18. Critical deformation of all five models is illustrated in Fig. 19 and 20. In the Fig. 19 we can see deformations of all models just in last moment before their collapses (last moment when they were stable), and in the Fig. 20 there is the deformation of models in the first moment just after the collapse.

TABLE I. VALUES OF CRITICAL COMPRESSION

" h " size [mm]	Critical compression [mm]
0.4	53
0.6	52
0.8	50
1.0	38
1.8	23

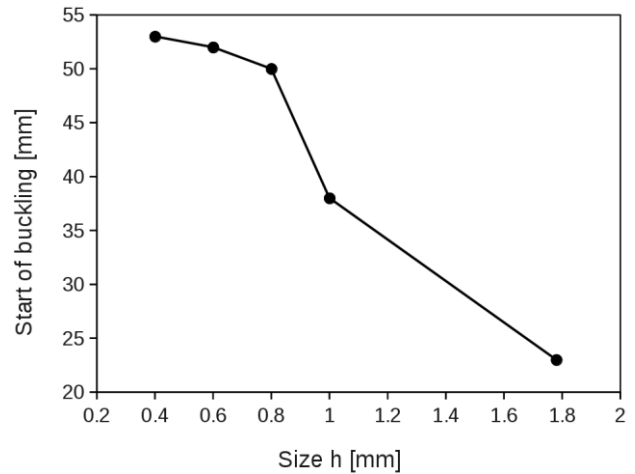


Fig. 18 dependence of boot stability on the h size

In case of dimension $h=0.4$ mm the model becomes (contrary to the reality) unstable, but nevertheless it is clear that this occurs almost at full compression of the boot. The difference between reality and the model is given by the size of each FEM element in the boot folds of model where we are not able to exactly copy arcs with such a small radius. But still we can say that the model is with good agreement with reality, it is able almost of full compression and thus it is sufficient for our analysis.

The second reference model ($h=1.8$ mm) collapses (contrary the previous model) already at low compression of 23 mm. Comparing Fig. 3 with Fig. 17 we can see that the model behaves exactly like the real product and collapses into identical shape.

The results of these two models show significant agreement with the reality and confirm suitability of the chosen methods for evaluating the influence of the boot profile shape (size h) on the stability of the boot during compression.

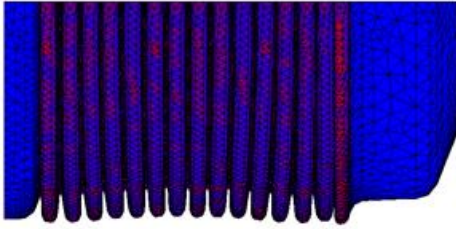
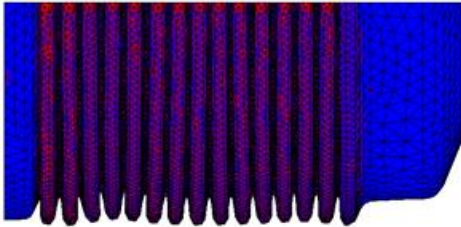
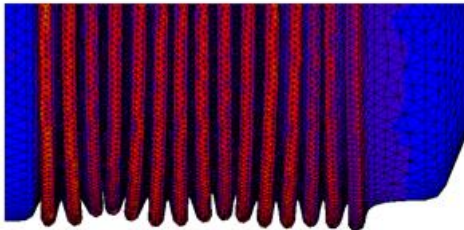
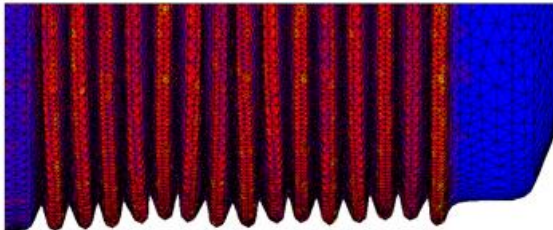
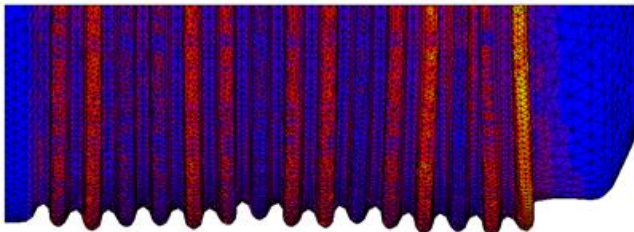
(a) $h = 0.4$ mm(b) $h = 0.6$ mm(c) $h = 0.8$ mm(d) $h = 1.0$ mm(e) $h = 1.8$ mm

Fig. 19 critical deformation of FEM models in the moment before the collapse

IV. CONCLUSION

It was obvious that with increasing size h boot stability will decrease, it means, the value of compression at which boot collapses will be reduced. However, strongly non-linear relation between h size and compression value (which is shown in Fig. 18) is very interesting.

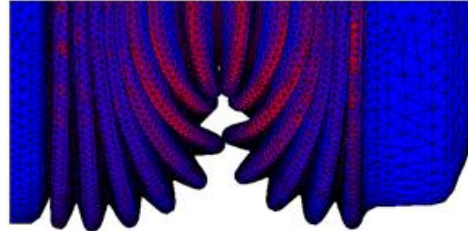
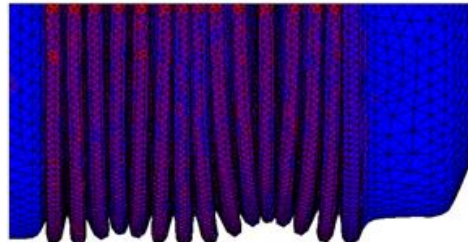
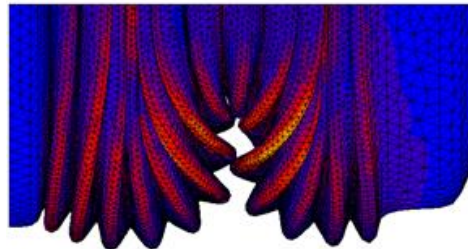
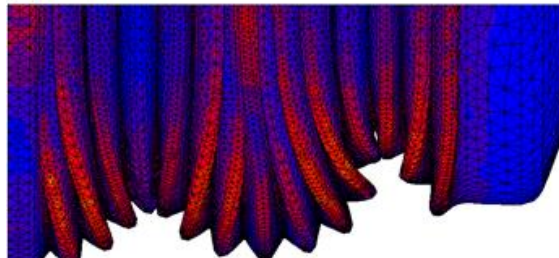
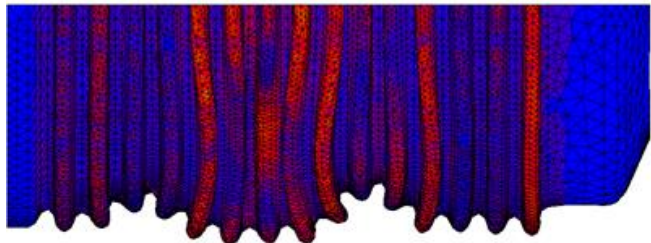
(a) $h = 0.4$ mm(b) $h = 0.6$ mm(c) $h = 0.8$ mm(d) $h = 1.0$ mm(e) $h = 1.8$ mm

Fig. 20 critical deformation of FEM models in the moment after the collapse

We can see a significant difference in stability between the boot with $h = 1.0$ mm and $h = 0.8$ mm. Additional reducing of the h still improves boot stability, but increase of the compression value is not as significant as in previous models. The results lead to the conclusion that the decisive factor is the ratio between the h size and the profile thickness in straight sections (which in our case is just 1 mm). The above results

show that the ratio of h / thickness = 0.8 / 1 should be sufficient for the proper function of the product.

REFERENCES

- [1] J. Javorik, M. Stanek, "The Shape Optimization of the Pneumatic Valve Diaphragm," *International Journal of Mathematics and Computers in Simulation*, vol. 5, pp. 361–369, 2011.
- [2] J. Javorik, M. Stanek, "The Numerical Simulation of the Rubber Diaphragm Behavior," in *Recent Researches in Automatic Control : 13th WSEAS International Conference on Automatic Control, Modelling & Simulation*, Lanzarote, Spain: WSEAS Press, 2011, pp. 117–120.
- [3] L. J. Billings, R. Shepherd, "The Modeling of Layered Steel/Elastomer Seismic Base Isolation Bearings," in *Proc. 1992 MARC User Conference*, Monterey, CA, USA, 1992.
- [4] M. C. Popescu, M. E. Mastorakis, "Optimal Flow Control of a Three Tank System," *International Journal of Mathematics and Computers in Simulation*, issue 4, vol. 3, pp. 179–186, 2009.
- [5] A. Arghiropol, C. Rotaru, "Overview of the 2D and 3D Finite Element Studies versus Experimental Results of a Solid Propellant Engine Performances under Cycling Loading Effect," *International Journal of Mathematics and Computers in Simulation*, vol. 4, pp. 42–49, 2010.
- [6] S. Amornsamankul, K. Kaorapapong, B. Wiwatanapataphee, "Three-Dimensional Simulation of Femur Bone and Implant in Femoral Canal using Finite Element Method," *International Journal of Mathematics and Computers in Simulation*, issue 4, vol. 4, pp. 171–178, 2010.
- [7] O. Suba, L. Sykorova, "Transient of Thermal Stresses in Printed Circuit Boards," *International Journal of Mechanics*, vol. 5, pp. 226–233, 2011.
- [8] L. Sykorova, O. Suba, "The Transient Temperature Field Simulation of Polymeric Materials During Laser Machining," *International Journal of Mechanics*, vol. 5, pp. 234–241, 2011.
- [9] M. Stanek, D. Manas, M. Manas, O. Suba, "Optimization of Injection Molding Process," *International Journal of Mathematics and Computers in Simulation*, vol. 5, pp. 413–421, 2011.
- [10] M. Stanek, D. Manas, M. Manas, J. Javorik, "Simulation of Injection Molding Process by Cadmould Rubber," *International Journal of Mathematics and Computers in Simulation*, vol. 5, pp. 422–429, 2011.
- [11] O. Suba, L. Sykorova, S. Sanda, M. Stanek, "Modeling of Thermal Stress in Printed Circuit Boards," in *Recent Researches in Automatic Control : 13th WSEAS International Conference on Automatic Control, Modelling & Simulation*, Lanzarote, Spain: WSEAS Press, 2011, pp. 173–176.
- [12] O. Suba, L. Sykorova, S. Sanda, M. Stanek, "Stress-State Modelling of Injection-molded Cylindrical Bosses Reinforced with Short Fibers," in *Recent Researches in Automatic Control : 13th WSEAS International Conference on Automatic Control, Modelling & Simulation*, Lanzarote, Spain: WSEAS Press, 2011, pp. 177–179.
- [13] L. Sykorova, O. Suba, M. Malachova, J. Cerny, "Temperature Field Simulation of Polymeric Materials During Laser Machining Using CASMOS/M Software," in *Recent Researches in Automatic Control : 13th WSEAS International Conference on Automatic Control, Modelling & Simulation*, Lanzarote, Spain: WSEAS Press, 2011, pp. 180–184.
- [14] M. Stanek, D. Manas, M. Manas, J. Javorik, "Simulation of injection molding process," in *Recent Researches in Automatic Control : 13th WSEAS International Conference on Automatic Control, Modelling & Simulation*, Lanzarote, Spain: WSEAS Press, 2011, pp. 231–234.
- [15] M. Stanek, D. Manas, M. Manas, O. Suba, "Optimization of injection molding process by MPX," in *Recent Researches in Automatic Control : 13th WSEAS International Conference on Automatic Control, Modelling & Simulation*, Lanzarote, Spain: WSEAS Press, 2011, pp. 212–216.
- [16] M. S. Salleh, M. Z. Omar, J. Syarif, M. N. Mohammed, K. S. Alhawari, "Thermodynamic Simulation on Thixoformability of Aluminium Alloys for Semi-solid Metal Processing," *International Journal of Mathematics and Computers in Simulation*, vol. 7, pp. 286–293, 2013.
- [17] D. Threadingham, W. Obrecht, W. Wieder, G. Wachholz, R. Engehausen, *Ullmann's Encyclopedia of Industrial Chemistry*. Wiley, 2011.
- [18] J. E. Mark, B. Erman, F. R. Eirich, *Science and Technology of Rubber*. Academic Press, 1994.
- [19] R. W. Ogden, *Non-linear Elastic Deformations*, New York, Dover Publications, 1997.
- [20] A. F. Bower, *Applied Mechanics of Solids*, New York, CRC Press, 2009.
- [21] A. N. Gent, "Extensibility of Rubber under Different Types of Deformation," *Journal of Rheology*, vol. 49, pp. 271–275, 2005.
- [22] P. Haupt, A. Lion, "On Finite Linear Viscoelasticity of Incompressible Isotropic materials," *Acta Mechanica*, vol. 159, pp. 87–124, 2002.
- [23] N. Huber, C. Tsakmakis, "Finite Deformation Viscoelasticity Laws," *Mechanics of Materials*, vol. 32, pp. 1–18, 2000.
- [24] J. E. Mark, "Rubber Elasticity," *Rubber Chemistry and Technology*, vol. 55, pp. 1123–1136, 1982.
- [25] L. R. G. Treloar, "Mechanics of Rubber Elasticity," *Journal of Polymer Science, Part C, Polymer Symposia*, vol. 48, pp. 107–123, 1974.
- [26] L. R. G. Treloar, *The Physics of Rubber Elasticity*, Clarendon Press, 1975.
- [27] A. Boukamel, L. Laiarinandrasana, S. Méo, E. Verron, *Constitutive Models for Rubber V*, London, Taylor & Francis, 2008.
- [28] M. C. Boyce, "Direct Comparison of the Gent a the Arruda-Boyce Constitutive Models of the Rubber Elasticity," *Rubber Chemistry and Technologies*, vol. 69, pp. 781–785, 1996.
- [29] R. A. Brockman, "On the Use of the Blatz-Ko Constitutive Model for Nonlinear Finite Element Analysis," *Computers and Structures*, vol. 24, pp. 607–611, 1986.
- [30] S. Govindjee, J. C. Simo, "A Micro-Mechanically Based Continuum Damage Model for Carbon Black Filled Rubbers Incorporating Mullins' Effect," *Journal of the Mechanics and Physics of Solids*, vol. 39, pp. 89–112, 1991.
- [31] A. Vandenbroucke, H. Laurent, N. Ait Hocine, G. Rio, "Hyperelasto-visco-hysteresis Model for an Elastomeric Behaviour: Experimental and Numerical Investigation," *Computational Materials Science*, vol. 48, pp. 495–503, 2010.
- [32] L. M. Yang, V. P. W. Shim, "A Visco-hyperelastic Constitutive Description of Elastomeric Foam," *International Journal of Impact Engineering*, vol. 30, pp. 1099–1110, 2004.
- [33] A. E. Zuniga, M. F. Beatty, "A New Phenomenological Model for Stress-softening in Elastomers," *Zeitschrift für Angewandte Mathematik und Physik*, vol. 53, pp. 794–814, 2002.
- [34] G. A. Holzapfel, *Nonlinear Solid Mechanics*, Wiley, 2000.
- [35] R. S. Rivlin, K. N. Sawyers, "Strain-energy Function for Elastomers," *Transaction of the Society of Rheology*, vol. 20, pp. 545–557, 1976.
- [36] M. H. B. M. Shariff, "Strain Energy Function for Filled and Unfilled Rubberlike Material," *Rubber Chemistry and Technology*, vol. 73, pp. 1–21, 2000.
- [37] R. H. Finney, A. Kumar, "Development of Material Constants for Nonlinear Finite Element Analysis," *Rubber Chemistry and Technology*, vol. 61, pp. 879–891, 1988.
- [38] A. N. Gent, *Engineering with Rubber*, Hanser, 2001.
- [39] W. D. Kim et al, "Some Considerations on Mechanical Testing Methods of Rubbery Materials Using Nonlinear Finite Element Analysis," *Polymer International*, vol. 53, pp. 850–856, 2004.
- [40] L. Chevalier, Y. Marco, "Tools for Multiaxial Validation of Behavior Lows Chosen for Modeling Hyperelasticity of Rubber-like Materials," *Polymer Engineering and Science*, vol. 42, pp. 280–298, 2002.
- [41] J. Javorik, Z. Dvorak, "The Testing of Hyperelastic Properties of the Rubber Materials," *Chemické listy*, vol. 105, pp. 273–274, 2011.
- [42] L. P. Smith, *The language of Rubber*, Oxford, Butterworth-Heinemann, 1993.
- [43] J. E. Mark, "Some Unusual Elastomers and Experiments on Rubberlike Elasticity," *Progress in Polymer Science*, vol. 28, pp. 1205–1221, 2003.
- [44] N. Reuge, F. M. Schmidt, Y. Le Maout, M. Rachik, F. Abbe, "Elastomer Biaxial Characterization Using Bubble Inflation technique. I: Experimental Investigations," *Polymer Engineering and Science*, vol. 41, pp. 522–531, 2001.
- [45] J. Javorik, Z. Dvorak, "Equibiaxial test of elastomers," *KGK – Kautschuk Gummi Kunststoffe*, vol. 60, pp. 608–610, 2007.
- [46] E. M. Arruda, M. C. Boyce, "A Three-Dimensional Constitutive Model for the Large Stretch Behavior of Rubber Elastic Materials," *Journal of the Mechanics and Physics of Solids*, vol. 41, pp. 389–412, 1993.

- [47] A. N. Gent, "A New Constitutive Relation for Rubber," *Rubber Chemistry and Technology*, vol. 69, pp. 781-785, 2001.
- [48] R. S. Rivlin, "Finite Elasticity Theory as a Model in the Mechanics of Viscoelastic Materials," *Journal of Polymer Science, Part C, Polymer Symposia*, vol. 48, pp. 125-144, 1974.
- [49] O. H. Yeoh, "Characterization of Elastic Properties of Carbon Black Filled Rubber Vulcanizates," *Rubber Chemistry and Technology*, vol. 63, pp. 792-805, 1990.
- [50] O. H. Yeoh, "Some Forms of the Strain Energy Function for Rubber," *Rubber Chemistry and Technology*, vol. 66, pp. 754-771, 1993.